The Astrophysical Journal Letters, 864:L22 (6pp), 2018 September 1 https://doi.org/10.3847/2041-8213/aadc10

RELICS: A Candidate $z \sim 10$ Galaxy Strongly Lensed into a Spatially Resolved Arc

Brett Salmon[1], Dan Coe[1], Larry Bradley[1], Marusa Bradač[2], Victoria Strait[2], Rachel Paterno-Mahler[3], Kuang-Han Huang[2], Pascal A. Oesch[4], Adi Zitrin[5], Ana Acebron[5], Nathália Cibirka[5], Shotaro Kikuchihara[6,7], Masamune Oguri[7,8,9], Gabriel B. Brammer[1], Keren Sharon[3], Michele Trenti[10], Roberto J. Avila[1], Sara Ogaz[1], Felipe Andrade-Santos[11], Daniela Carrasco[10], Catherine Cerny[3], William Dawson[12], Brenda L. Frye[13], Austin Hoag[2], Christine Jones[11], Ramesh Mainali[13], Masami Ouchi[6,8], Steven A. Rodney[14], Daniel Stark[13], and Keiichi Umetsu[15]

[1] Space Telescope Science Institute, Baltimore, MD, USA; bsalmon@stsci.edu
[2] Department of Physics, University of California, Davis, CA 95616, USA
[3] Department of Astronomy, University of Michigan, 1085 South University Avenue, Ann Arbor, MI 48109, USA
[4] Geneva Observatory, University of Geneva, Ch. des Maillettes 51, 1290 Versoix, Switzerland
[5] Physics Department, Ben-Gurion University of the Negev, P.O. Box 653, Beer-Sheva 84105, Israel
[6] Institute for Cosmic Ray Research, The University of Tokyo, 5-1-5 Kashiwanoha, Kashiwa, Chiba 277-8582, Japan
[7] Department of Physics, Graduate School of Science, The University of Tokyo, 7-3-1 Hongo, Bunkyo-ku, Tokyo 113-0033, Japan
[8] Kavli Institute for the Physics and Mathematics of the Universe (Kavli IPMU, WPI), University of Tokyo, Chiba 277-8582, Japan
[9] Research Center for the Early Universe, The University of Tokyo, 7-3-1 Hongo, Bunkyo-ku, Tokyo 113-0033, Japan
[10] School of Physics, University of Melbourne, VIC 3010, Australia
[11] Harvard-Smithsonian Center for Astrophysics, 60 Garden Street, Cambridge, MA 02138, USA
[12] Lawrence Livermore National Laboratory, P.O. Box 808 L- 210, Livermore, CA, 94551, USA
[13] Department of Astronomy, Steward Observatory, University of Arizona, 933 North Cherry Avenue, Rm N204, Tucson, AZ, 85721, USA
[14] Department of Physics and Astronomy, University of South Carolina, 712 Main Street, Columbia, SC 29208, USA
[15] Institute of Astronomy and Astrophysics, Academia Sinica, P.O. Box 23-141, Taipei 10617, Taiwan
Received 2018 January 9; revised 2018 August 15; accepted 2018 August 17; published 2018 August 31

Abstract

The most distant galaxies known are at $z \sim 10$–11, observed 400–500 Myr after the Big Bang. The few $z \sim 10$–11 candidates discovered to date have been exceptionally small, barely resolved, if at all, by the *Hubble Space Telescope*. Here we present the discovery of SPT0615-JD1, a fortuitous $z \sim 10$ ($z_{\rm phot} = 9.9^{+0.8}_{-0.6}$) galaxy candidate stretched into an arc over $\sim 2\farcs5$ by the effects of strong gravitational lensing. Discovered in the Reionization Lensing Cluster Survey (RELICS) *Hubble* Treasury program and companion S-RELICS *Spitzer* program, this candidate has a lensed H-band magnitude of 24.6 ± 0.1 AB mag. With a magnification of $\mu \sim 4$–7 estimated from our lens models, the delensed intrinsic magnitude is 26.7 ± 0.1 AB mag, and the half-light radius is $r_e < 0.8$ kpc, both consistent with other $z > 9$ candidates. The inferred stellar mass ($\log[M_\star/M_\odot] = 8.3^{+0.3}_{-0.2}$) and star formation rate ($\log[{\rm SFR}/M_\odot\ {\rm yr}^{-1}] = 1.1^{+0.5}_{-0.4}$) indicate that this candidate is a typical star-forming galaxy on the $z > 6$ SFR–$M_\star$ relation. We note that three independent lens models predict two counter images, at least one of which should be of a similar magnitude to the arc, but these counter images are not yet detected. Counter images would not be expected if the arc were at lower redshift. The relatively large physical size could be due to a merger or accretion event, while the unprecedented lensed size of this $z \sim 10$ candidate offers the potential for *ALMA* and the *James Webb Space Telescope* to study the geometric and kinematic properties of a galaxy observed 500 Myr after the Big Bang.

Key words: galaxies: clusters: general – galaxies: evolution – galaxies: high-redshift – gravitational lensing: strong

1. Introduction

With its high resolution and sensitivity, observations using the *Hubble Space Telescope* (*HST*) have sharpened our understanding of the high-z universe. Deep and wide extra-galactic imaging surveys with ACS and WFC3 have uncovered thousands of galaxies at $z > 6$ in blank fields (see Finkelstein 2016; Stark 2016, for reviews), including the most distant galaxy found to date at $z = 11.1$ (GN-z11; Oesch et al. 2016). In addition, we have prioritized the *HST* to observe the most massive galaxy clusters, taking advantage of the natural telescopes they create via strong gravitational lensing (CLASH, PI: Postman; Frontier Fields, PI: Lotz; RELICS, PI: Coe). This investment in lensing fields has proven fruitful. We have discovered highly magnified (MACS1149-JD, Zheng et al. 2012; Hoag et al. 2017; MACS1115-JD and MACS1720-JD, Bouwens et al. 2014; MACS0416-JD, Infante et al. 2015) and multiply imaged galaxies (MACS0647-JD, Coe et al. 2013; A2744-JD, Zitrin et al. 2014) at redshifts up to $z \sim 10.8$, which have allowed us to study faint UV metal lines (Stark et al. 2014; Rigby et al. 2015; Mainali et al. 2017), nebular emission lines (Stark et al. 2015; Laporte et al. 2017; Smit et al. 2017), and the star formation rate (SFR) density deep into the epoch of reionization (Oesch et al. 2014, 2018).

However, little is known in detail about the $z > 9$ universe, and the handful of candidates found so far exhibit peculiar properties. At $z \sim 11$, MACS0647-JD has a radius smaller than 100 pc, the size of giant molecular clouds in the local universe. GN-z11 is three times brighter than the characteristic UV luminosity (L_*) of galaxies at that distance, surprisingly bright given the CANDELS search area. Both $z \sim 9$ and ~ 10 candidates MACS1149-JD and MACS0416-JD (the former spectroscopically confirmed; Hashimoto et al. 2018) appear to have evolved stellar populations of $\approx$300 Myr, when the age of the universe was only $\approx$500 Myr. *JWST* NIRCam will better sample the rest-frame UV-to-optical colors which will break some parameter degeneracies and challenge these initial inferences. However, with typical $z \sim 10$ effective radii of

$<0\farcs2$ and a NIRCAM PSF FWHM[16] of $\sim0\farcs05$ at 1.5 μm, it will still be difficult resolve these galaxies spatially. Ideally, we can use the help of strong lensing to study the kinematics and intrinsic stellar populations at $z \sim 10$ in detail.

In this Letter we present a galaxy gravitationally lensed into an arc with a photometric redshift of $z_{\rm phot} = 9.9 \pm 0.6$. Discovered in the Reionization Lensing Cluster Survey (RELICS) *Hubble* (*HST*) and *Spitzer Space Telescope* imaging, the arc features of this candidate extend across $\sim2\farcs5$, allowing unprecedented physical resolution deep in the epoch of reionization. This new candidate has an *HST* F160W *H*-band magnitude of $H = 24.6 \pm 0.1$ AB, bright enough for follow-up spectroscopic or grism observations. In this work, we present the physical characteristics of this candidate and discuss the supporting evidence of its high redshift. Throughout, we assume concordance cosmology with $H_0 = 70\,{\rm km\,s^{-1}\,Mpc^{-1}}$, $\Omega_{\Lambda,0} = 0.7$, and $\Omega_{\rm M,0} = 0.3$.

2. Data and Photometry

2.1. Cluster Field and HST Photometry

The galaxy cluster SPT-CL J0615-5746 (hereafter SPT0615-57; also known as PLCK G266.6-27.3) was discovered independently by the South Pole Telescope survey (SPT; Williamson et al. 2011) and Planck Collaboration et al. (2011). It is exceptionally massive ($M_{500} = 7.1 \times 10^{14}\,M_\odot$) for its high redshift ($z = 0.972$). The SPT and Planck teams obtained *HST* imaging (GO 12477 and 12757) of the cluster with the ACS/WFC F606W filter *V* (one-orbit depth) and F814W filter *I* (combined two-orbit depth). RELICS (GO 14096) obtained ACS/WFC imaging (1 orbit) in F435W *B* and WFC3/IR imaging (two orbits) in F105W *Y*, F125W *J*, F140W *JH*, and F160W *H*.

RELICS obtained similar *HST* imaging with WFC3/IR and ACS on a total of 41 clusters. The details of the image reduction, SExtractor (version 2.8.6; Bertin & Arnouts 1996) object selection, and *HST* photometry are described by Salmon et al. (2017) and D. Coe et al. (2018, in preparation). SPT0615-57 is the highest redshift cluster and the second-highest producer of high-z candidates out of the 41 RELICS fields, revealing 25 new candidate galaxies over the redshift range $5.5 < z < 8.5$ (Salmon et al. 2017).

Table 1 shows the three $z > 9$ candidates found in RELICS after fitting photometric redshifts to *HST* data only. One of these candidates appears as a spatially resolved arc. Figure 1 shows image cutouts of this candidate, hereafter SPT0615-JD1 ("JD" for *HST* F125W *J*-band dropout). The initial SExtractor segmentation map did not cover the entirety of the arc, so we additionally performed aperture photometry on the *HST* images of this candidate (elliptical aperture $a = 1\farcs8$, $b = 0\farcs35$, at an angle $\theta = 135°$), and applied a local background subtraction. As described in Table 1, SPT0615-JD1 has an AB magnitude of 24.6 ± 0.1 in F160W detected with a single-to-noise ratio (S/N) $\sim$ 10 (the F160W exposures were in two epochs 44 days apart, each detecting the source with S/N $\sim$ 7). The extended arc shape is consistent with the direction of the lensing shear expected from the cluster (see Section 3). The bands blueward of F140W yield nondetections with S/N $\lesssim$ 1, and F140W and F160W are both detected (S/N = 5.0 and 10.1, respectively). Importantly, we emphasize that the observed-frame size of SPT0516-JD is large ($\sim2\farcs5$ long), and can easily be spatially resolved by *JWST* (see Section 5).

Table 1
RELICS $z \sim 10$ Candidate and $z \sim 3$ Interlopers

Field	SPT0615-57	PLCKG138-10	RXC0018+16
RELICS ID	336	748	1107
α_{J2000}	06:15:55.03	02:27:00.86	00:18:33.84
δ_{J2000}	−57:46:19.56	49:00:22.68	16:25:18.84
B_{435}[a]	>27.2	>26.8	>28.8
V_{606}	>27.5	>28.4	>28.8
I_{814}	>28.1	>27.0	>29.4
Y_{105}	>27.1	>27.3	>28.4
J_{125}	>26.1	>26.5	>26.9
JH_{140}	24.8 ± 0.2	26.0 ± 0.2	>26.6
H_{160}	24.6 ± 0.1	25.2 ± 0.1	26.1 ± 0.1
[3.6 μm]	25.5 ± 0.4	23.4 ± 0.1	23.1 ± 0.1
[4.5 μm]	25.2 ± 0.3	22.9 ± 0.1	22.8 ± 0.1
$z_{\rm phot,HSTonly}$[b]	$9.6^{+0.7}_{-7.4}$	$10.0^{+0.6}_{-7.5}$	$9.9^{+0.7}_{-1.0}$
$z_{\rm phot,HST+Spitzer}$	$9.9^{+0.8}_{-0.6}$	$2.7^{+0.1}_{-0.1}$	$3.6^{+0.2}_{-0.2}$

Notes.
[a] We present 1σ upper limits for undetected bands.
[b] Photometric redshifts found using Bayesian photometric redshift (BPZ; Benítez 2000). The two $z \sim 3$ interlopers from PLCKG138-10 and RXC0018+16 were initially identified as $z \sim 10$ candidates prior to including the *Spitzer* data, whereas the candidate in SPT0615-57 remained at $z \sim 10$.

2.2. Spitzer Photometry

After finding the initial $z = 9$–10 candidates with *HST* data, we further vetted these candidates by checking *Spitzer* data from the S-RELICS programs (PI: Bradač; PI: Soifer) including a recent Cycle 13 DDT program to observe SPT0615-57. The IRAC channel 1 and 2 bands (3.6 and 4.5 μm, respectively, with current depths per band of $\approx$17 hr), correspond to rest-frame optical flux at $z \sim 9$–10 and are invaluable for distinguishing between intrinsically bluer $z \sim 10$ star-forming galaxies and intrinsically redder $z \sim 2$ interloper galaxies. The *Spitzer* fluxes were extracted using `T-PHOT` (Merlin et al. 2016) which uses the higher resolution *HST* imaging as a prior to extract photometry from the lower resolution *Spitzer* images. First, we produce point-spread function (PSF) convolution kernels based on all available *HST* images. We manually sharpen the PSF to minimize residuals between the convolved image and *Spitzer* images. Then, we run `T-PHOT` on a localized region around the existing WFC3/IR imaging as opposed to the entire cluster field, which we have found produces cleaner residuals, indicating a more reliable source extraction. After obtaining the *Spitzer* photometry and recalculating photometric redshifts, we rule out two candidates as low-z interlopers, leaving SPT0615-JD1 as the only $z \sim 10$ candidate.

We note that Figure 1 also reveals an IR-bright nearby $z \sim 3$ galaxy. `T-PHOT` reports a high maximum covariance between the photometry of SPT0615-JD1 and its bright northwest neighbor. To test our ability to accurately determine *Spitzer* fluxes, we conducted an input/output photometry simulation. First, we used elliptical apertures to extract the images of JD1 and its bright neighbor from the F160W image. Next, we manually scaled their fluxes and convolved them with the *Spitzer* PSF. We then pasted each of these two new sources into a clear, nearby region of the real 3.6 μm image. We calculated the fluxes of the new sources in a blind experiment where the investigator running `T-PHOT` did not know the true input flux

[16] see https://jwst-docs.stsci.edu.

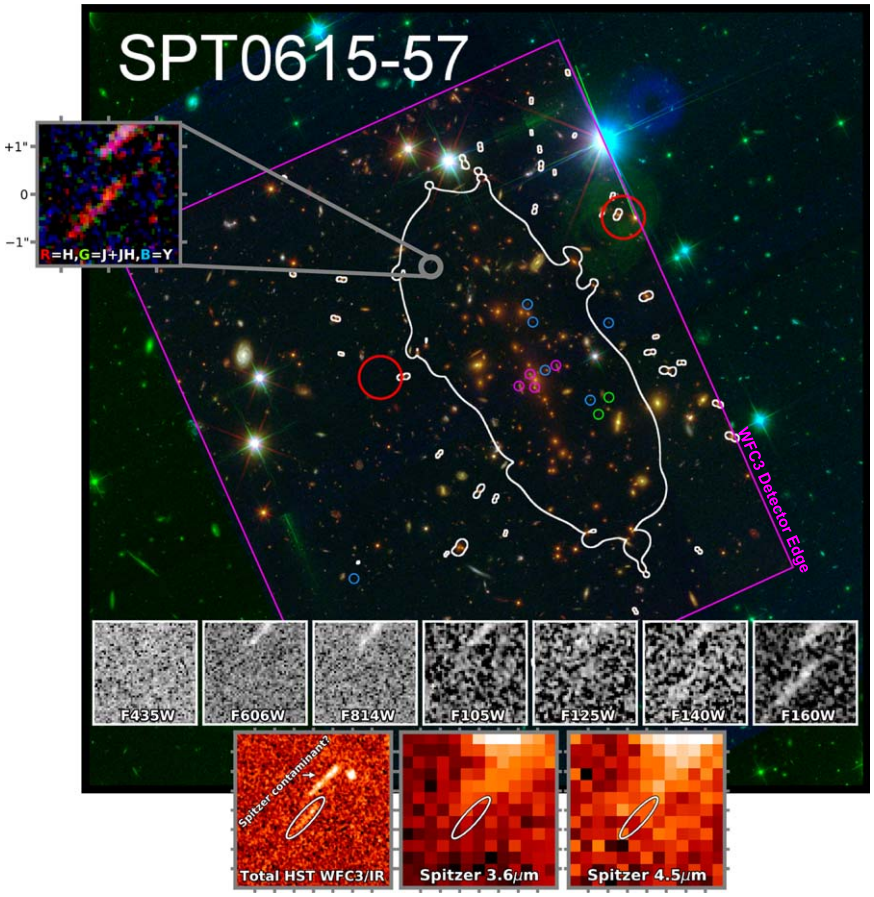

Figure 1. $3\farcm25 \times 3\farcm25$ color image of the *HST* RELICS cluster field SPT0615-57. The yellow circle marks the location of the $z \sim 10$ candidate SPT0615-JD1. The white lines and large red circles show the $z = 10$ critical curves and predicted locations of the yet undetected counter images from the Paterno-Mahler et al. (2018) lens model. The small green and magenta circles show the positions of the two sets of multiple images used in their primary lens model, and the blue circles mark a set used in a lower likelihood model. The violet lines mark the edge where WFC3/IR data is available. The expanded inset is a $3'' \times 3''$ WFC3/IR RGB color image with the R channel as F160W, G as the sum of F125W and F140W, and B as F105W. The bottom row of insets are the ACS images followed by WFC3/IR images, all $3'' \times 3''$ and 60 mas resolution. The candidate is nondetected in the bands blueward of F140W, indicating a strong spectral break. Bottom row: larger $8'' \times 8''$ cutouts with ellipses marking the position of SPT0615-JD1. Bottom left, right, and middle: A weighted stack of all four WFC3/IR bands centered on SPT0615-JD1, and the *Spitzer* 3.6 and 4.5 μm images. The *Spitzer* flux from the nearby bright $z \sim 3$ galaxy crowds the $z \sim 10$ candidate, which appears otherwise faint.

scalings. Finally, we compared the input and output fluxes and repeated the experiment 40 times for several input flux combinations and source locations.

We found that we are only able to accurately recover lensed magnitudes brighter than [3.6 μm] $\approx$ 24.5 mag for JD1, given its proximity to the brighter galaxy. For fainter simulated sources (including zero flux), our methods yield spurious magnitude measurements of $\approx$25 mag due to light from the neighboring galaxy. Given the relatively faint observed magnitude (Table 1, [3.6 μm] $= 25.5 \pm 0.4$), we conclude that SPT0615-JD1 is not significantly brighter than its observed magnitude at 3.6 and 4.5 μm, but could be fainter.

Even assuming a conservatively higher magnitude (e.g., [3.6 μm] = 24), the H$-$[3.6 μm] color is still several magnitudes lower than typical low-z interlopers. This is critical because while all $z \sim 10$ solutions could have lower *Spitzer* fluxes, the low-z solution *requires* them to be high. For a low-z spectral energy distribution (SED) to match the extreme red slope in the *HST* IR bands, it must have a high dust attenuation and therefore red F160W$-$[3.6 μm] and [3.6 μm]$-$[4.5 μm] colors, i.e., several magnitudes brighter in *Spitzer*. Conversely, the *Spitzer* bands sample rest-frame optical light for a high-z source, and the red slope in the *HST* bands is simply caused by the Lyman break. Our tests with BPZ show that the $z < 8$ probability will only each >5% when the lensing-corrected [3.6 μm] and [4.5 μm] magnitudes are >24.5 mag (>23 mag lensed), with the current *HST* photometry. Even adopting the upper-limit magnitude from our simulations (observed [3.6 μm] $\approx$ 24.5, and assuming the same red color as seen in the data of [3.6 μm]$-$[4.5 μm] = 0.32 mag), and a low lensing magnification ($\mu = 4$, such that the object is intrinsically brighter, thus increasing low-z likelihood due to magnitude priors) the total $z < 8$ probability is still $\ll$1%.

3. Lens Models

Figure 1 shows three sets of multiply imaged galaxies: two with spectroscopic redshifts ($z = 1.358$ and $z = 4.013$) and one whose redshift is free to vary in the modeling. We use these sources to produce three independent lens models using `Lenstool` (see Paterno-Mahler et al. 2018, hereafter PM18), `GLAFIC` (Oguri 2010), and the Zitrin et al. (2015) light-traces-mass (LTM) method. PM18 estimate the magnification of SPT0615-JD1 to be $\mu \sim$ 4–7, and we adopt the upper end magnification throughout this work.

All three models predict two counter images at the positions shown in Figure 1. Our results using `GLAFIC` (S. Kikuchihara et al. 2018, in preparation) and `Lenstool` (PM18) predict that

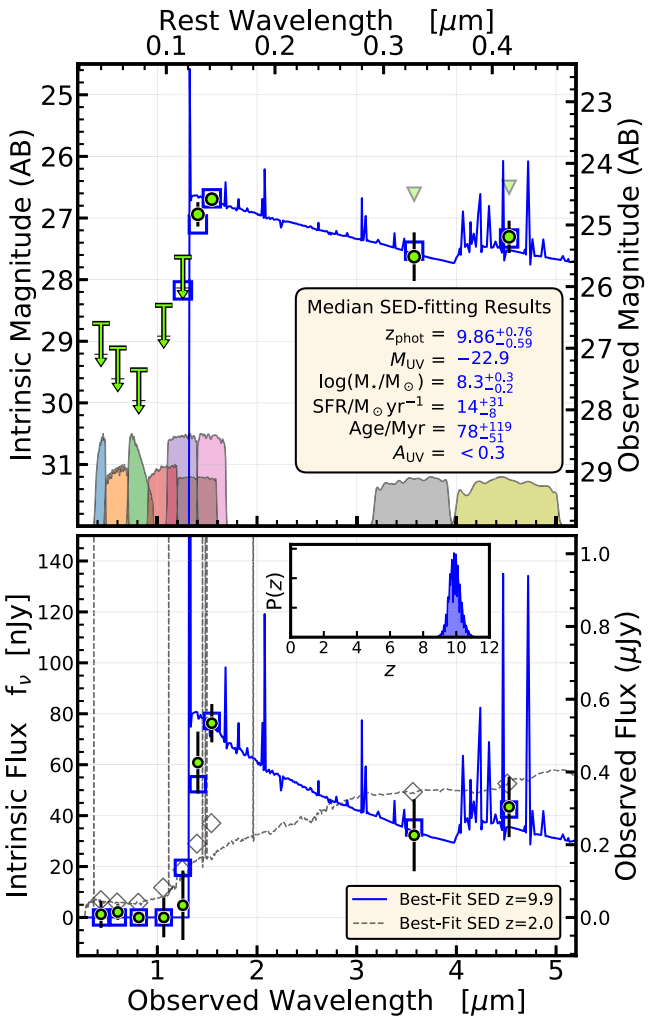

Figure 2. Best-fit SEDs to RELICS *HST* and *Spitzer* photometry (green circles) of SPT0615-JD1. The solid blue line and squares (dotted gray line and diamonds) show the best-fit SED and model fluxes, respectively, assuming the $z \sim 10$ ($z \sim 2$) solution. The top (bottom) plot displays the observed and lensing-corrected magnitudes (fluxes), the latter assuming a magnification of $\mu = 7$. Downward triangles show the *Spitzer* magnitude upper limits derived from photometry simulations (see Section 2). The top plot also shows the *HST* and *Spitzer* transmission curves for reference. Fluxes have been corrected for lensing magnification. The lower inset figure shows the redshift likelihood, $P(z)$, which strongly favors the $z \sim 10$ solution, with <1% likelihood for any $z < 6$ solution.

the northwest counter image is ≈1 mag fainter than the original arc, and therefore below the detection limit, or else potentially out of the field of view of the current WFC3/IR imaging. All three models predict the southeast counter image to be of similar magnification and magnitude of the original arc, and LTM predicts the counter images to have the same magnitude as the original arc. Given these models, we would have expected to see an image near the southeast position, but none are yet detected. Given the current shallow WFC3/IR depths (∼26 mag in F160W), there still exist several explanations for the nondetection of the southeast counter image. For example, it would be below the detection limit if we assume the lowest end of the magnification estimates from PM18 ($\mu = 2.5$). In addition, "model 3" from PM18 ($\chi_\nu = 0.96$, which uses the less-secure arcs labeled blue in Figure 1) does not predict a southeast counter image, but this is not the best-fitting model from their work. Conversely, all lens models predict no counter images if SPT0615-JD1 is at $z \sim 2$. Deeper imaging of this field is required to properly search for the $z \sim 10$ counter images and yield geometric support as in Coe et al. (2013), Zitrin et al. (2014), and Chan et al. (2017).

4. SED Fitting

Thanks to the *Spitzer* data that probes the rest-frame optical and near-UV (∼2900–4500 Å), we can infer upper limits on physical parameters like stellar mass and dust attenuation to test if the high- and low-z solutions are sensible. We use a Bayesian SED-fitting procedure originally described by Papovich et al. (2001) and updated by Salmon et al. (2015). In short, we sample the posterior using a grid of SEDs that represent a range of stellar population ages ($10\,\mathrm{Myr} < t_{\rm age} < t_{\rm universe}$, logarithmically spaced), attenuation ($0 < A_{\rm UV} < 7.4$), metallicity ($0.02\,Z_\odot < Z < Z_\odot$), and rising star formation histories ($\Psi(t) = \Psi_0 \exp(t/\tau_{\rm SFH})$, where the e-folding timescale $\tau_{\rm SFH}$ can be 0.3, 0.5, 0.7, 1, 3, 5, 7, 10, 30, 50, 70, or 100 Gyr). We use Bruzual & Charlot (2003) stellar population synthesis models with a Chabrier (2003) IMF17 and include the effects of nebular emission lines following Salmon et al. (2015). We assume the dust-attenuation law derived by Salmon et al. (2016) that varies in shape from a steep law at low attenuation (similar in shape to the extinction law of the small magellanic cloud) to a gray law at high attenuation (similar in shape to the starburst curve of Calzetti et al. (2000)).

The results of our SED fitting are summarized in Figure 2. For all SED fittings, we correct for lensing magnification assuming $\mu = 7$, and do not further correct the *Spitzer* fluxes despite likely contamination (see Section 2 and Figure 1). The fits assuming the $z \sim 10$ redshift show a moderately high stellar mass of $M_\star = 10^{8.3^{+0.3}_{-0.2}}\,M_\odot$ and SFR $= 14^{+31}_{-8}\,M_\odot\,\mathrm{yr}^{-1}$. The stellar mass and SFR of SPT0615-JD1 are indicative of a typical star-forming galaxy at $z \sim 10$ (Oesch et al. 2014) and would lie on the SFR-$M_\star$ relation at $z \sim 6$ (Salmon et al. 2015).

While the physical size of the candidate is large (see Section 5), its stellar mass and SFR indicate that it is a normal star-forming galaxy. The [3.6 μm]−[4.5 μm] *Spitzer* color, which straddles the rest-frame 4000 Å break, is modestly red, but not enough to produce evidence of evolved stellar populations (aged ≈300 Myr) like in other candidates (Hoag et al. 2017; Hashimoto et al. 2018).

5. Comparison with Other High-redshift Candidates

Figure 3 shows the H-band magnitude versus redshift for all high-z ($z > 5.5$) candidate galaxies discovered in RELICS (Salmon et al. 2017) and many other deep and wide surveys. The lensed, observed-frame size of SPT0615-JD1 stands out as spatially much larger than other $z \sim 10$ candidates (other candidates at these redshifts have similar point-like sizes to those found by Coe et al. 2013 and Oesch et al. 2016, see below). The intrinsic (delensed) magnitude of SPT0615-JD1 is similar to that of the $z \sim 11$ candidate MACS0647-JD (Coe et al. 2013).

An independent way to test high- and low-z solutions for SPT0615-JD1 is to calculate its physical size and compare to other known interlopers. Moreover, the sizes of galaxies can give us great physical insight into the initial conditions of early

[17] Switching from a Chabrier (2003) to a Salpeter (1955) IMF would result in higher derived stellar mass and SFR by 0.25 dex.

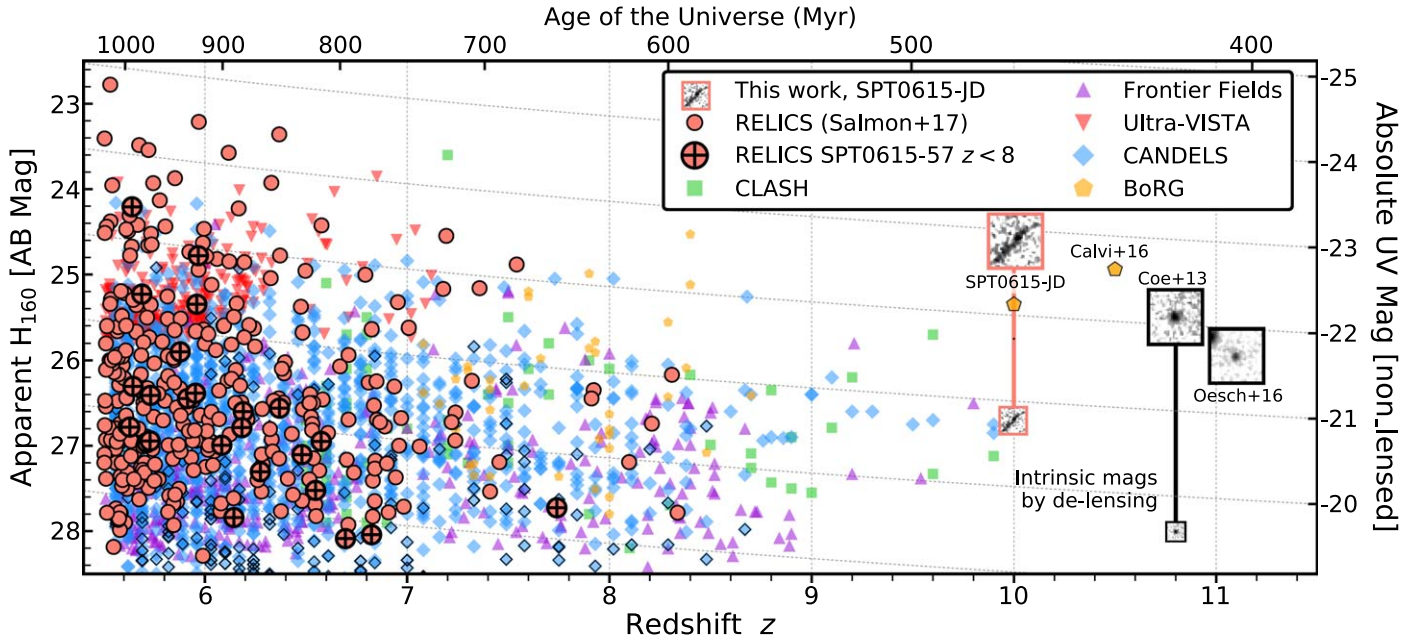

Figure 3. Observed H-band magnitude vs. redshift for $z > 5.5$ candidates from various surveys. The $z < 8.5$ candidates from Salmon et al. (2017) are shown as salmon-colored circles, and the candidates from SPT0615-57 are filled with crosses. The green squares are galaxies from CLASH (Zheng et al. 2012; Bradley et al. 2014; Hoag et al. 2017), purple upwards triangles from the Frontier Field (Zitrin et al. 2014; Ishigaki et al. 2018), red downwards triangles from Ultra-VISTA (Bowler et al. 2017), blue diamonds from CANDELS (Bouwens et al. 2014, 2015; Oesch et al. 2016; outlined diamonds are from the HUDF; see also Finkelstein et al. 2015), and orange pentagons from BoRG/HIPPIES (Bradley et al. 2012; Schmidt et al. 2014; Calvi et al. 2016). Gray lines follow the conversion from apparent to absolute UV magnitude to reference for unlensed sources. $2'' \times 2''$ cutout images of two $z \sim 11$ candidates (Coe et al. 2013; Oesch et al. 2016) and the $z \sim 10$ candidate from this work mark their observed magnitudes, respectively. For the latter two candidates, we also show their cutouts scaled in size according to their lens model to show an example of their intrinsic size (a full source-plane reconstruction of SPT0615-JD1 would show a smaller axis ratio). SPT0615-JD1 has a much larger observed size compared to the other candidates.

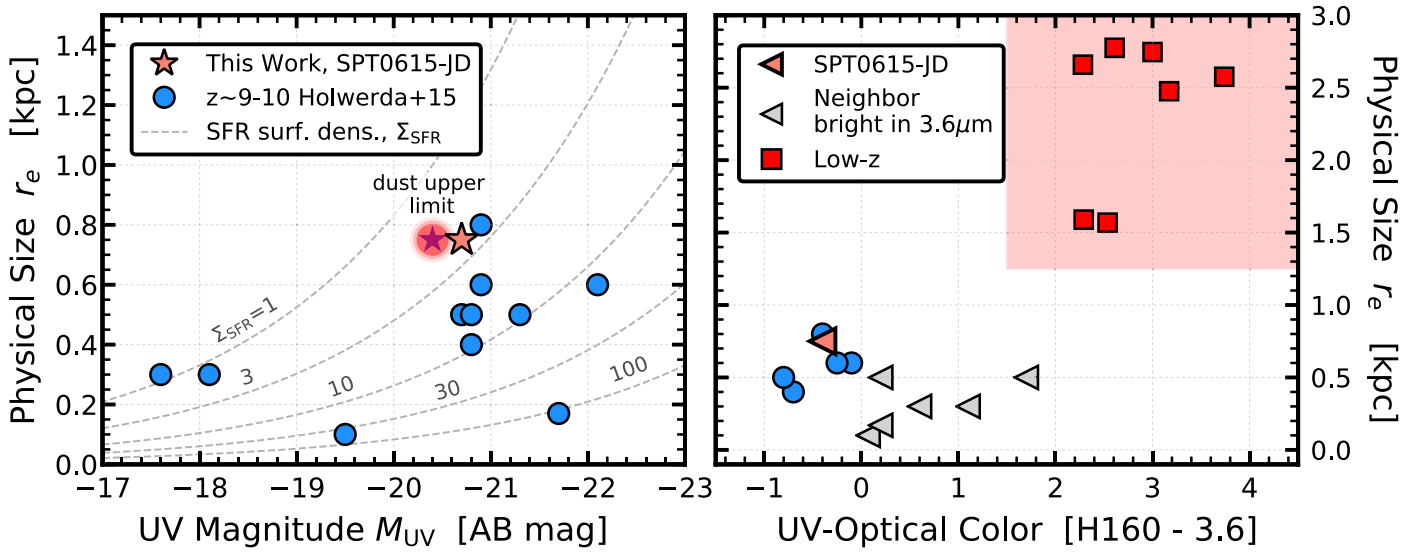

Figure 4. Size of SPT0615-JD1 compared to other known $z > 9$ galaxy candidates (blue circles). Left: the physical size (effective radius) as a function of absolute UV magnitude. The delensed magnitude is shown as the red circle and star, and the unobscured (corrected for our upper-limit dust extinction) delensed magnitude is shown as the salmon-colored star. Right: the physical size as a function of [F160W−3.6 μm] color. Triangles show $z > 9$ candidates, including SPT0615-JD1 (bold triangle), that may be contaminated in *Spitzer* flux by a bright neighbor, resulting in redder [F160W−3.6 μm] colors. Significantly larger sizes of typical very red $z \sim 2$ galaxies (red squares) are shown in the red box.

disk evolution (Ferguson et al. 2004). Broadly, the $z > 5$ size evolution at fixed luminosity scales as $(1+z)^{-m}$ where $m = 1$–2 (Shibuya et al. 2015). Holwerda et al. (2015) demonstrated that a combination of UV-to-optical color, sampled by the F160W and 3.6 μm bands, and physical size can be used to identify obvious low-z contaminants. They summarized that the sizes of $z > 9$ galaxy candidates have typical half-light radii of $r_e < 0.8$ kpc.

To calculate the size of SPT0615-JD1, we used our lens models to reconstruct its image in the source plane. The LTM lens model finds a relatively mild tangential magnification, or shear, of a factor of ∼3, leaving the full width of the delensed

source to be about 3–3.5 kpc. If we assume that the light distribution is uniform, we can take the half-light radius to be about $\sim 1/4$ of the full size and find $r_e \approx 0.7$–0.8 kpc. The statistical error on this size (from the lens model) is only a couple of percent, so we are dominated by systematic errors ($\sim$10%). Curiously, the reconstructed source's axis ratio is still about 2:1 in the same direction as the lensing shear, which could mean that the shear is underestimated and the size is in fact smaller.

Figure 4 shows that the inferred size of SPT0615-JD1 is typical compared to other high-z candidates. This provides crucial evidence in support of the $z \sim 10$ solution that is independent of the galaxy SED. While the uncertainty in the $z \sim 10$ UV dust attenuation should be considered as an upper limit, the candidate is still within the range of $M_{\rm UV}$ and SFR surface density of known $z > 9$ candidates.

6. Conclusions

We present SPT0615-JD1, a promising $z \sim 10$ galaxy candidate that appears to be stretched into the shape of an arc by the effects of strong gravitational lensing. Out of all combined lensing fields from RELICS, CLASH, and the Frontier Fields, there is no other galaxy candidate spatially stretched by lensing as distant as SPT0615-JD1. While our three independent lens models predict at least one detectable counter image, we do not see one in the current data. No counter images are expected if the candidate is at lower redshift. After deriving photometry from our deep *Spitzer* imaging, and validating our conclusions with recovery simulations, we conclude that SPT0615-JD1 is a typical star-forming galaxy at $z \sim 10$, with $<1\%$ likelihood for lower redshift solutions. Finally, we find that the source-plane size of SPT0615-JD1 is large, but comparable to other $z = 9$–10 galaxies, while the observed-frame image offers unprecedented spatial resolution. This large size could be due to a merger or accretion event, although higher resolution imaging is required to investigate further. This galaxy candidate offers the unique opportunity for resolving stellar populations deep in the epoch of reionization, especially with the greater sensitivity and higher resolution imaging of *JWST*.

This Letter uses observations from NASA/ESA *HST*. STScI is operated by AURA under NASA contract NAS 5-26555, ACS under NASA contract NAS 5-32864, and *Spitzer* by JPL. These observations are associated with program GO-14096 and archival data are associated with programs GO-12757 and GO-12477. Some data were obtained from MAST. The RELICS archive at MAST can be obtained at doi:10.17909/T9SP45. This work was performed under the auspices of the U.S. Department of Energy by LLNL under contract DE-AC52-07NA27344. F.A.-S. acknowledges support from Chandra grant G03-14131X.

ORCID iDs

Brett Salmon https://orcid.org/0000-0002-7453-7279
Dan Coe https://orcid.org/0000-0001-7410-7669
Larry Bradley https://orcid.org/0000-0002-7908-9284
Marusa Bradač https://orcid.org/0000-0001-5984-0395
Victoria Strait https://orcid.org/0000-0002-6338-7295
Rachel Paterno-Mahler https://orcid.org/0000-0003-3653-3741
Kuang-Han Huang https://orcid.org/0000-0001-7826-6448
Pascal A. Oesch https://orcid.org/0000-0001-5851-6649
Adi Zitrin https://orcid.org/0000-0002-0350-4488
Ana Acebron https://orcid.org/0000-0003-3108-9039
Nathália Cibirka https://orcid.org/0000-0002-2356-4680
Masamune Oguri https://orcid.org/0000-0003-3484-399X
Gabriel B. Brammer https://orcid.org/0000-0003-2680-005X
Keren Sharon https://orcid.org/0000-0002-7559-0864
Michele Trenti https://orcid.org/0000-0001-9391-305X
Felipe Andrade-Santos https://orcid.org/0000-0002-8144-9285
Daniela Carrasco https://orcid.org/0000-0002-3772-0330
William Dawson https://orcid.org/0000-0003-0248-6123
Austin Hoag https://orcid.org/0000-0001-8989-2567
Ramesh Mainali https://orcid.org/0000-0003-0094-6827
Masami Ouchi https://orcid.org/0000-0002-1049-6658
Steven A. Rodney https://orcid.org/0000-0003-1947-687X
Keiichi Umetsu https://orcid.org/0000-0002-7196-4822

References

Benítez, N. 2000, ApJ, 536, 571
Bertin, E., & Arnouts, S. 1996, A&AS, 117, 393
Bouwens, R. J., Bradley, L., Zitrin, A., et al. 2014, ApJ, 795, 126
Bouwens, R. J., Illingworth, G. D., Oesch, P. A., et al. 2015, ApJ, 803, 34
Bowler, R. A. A., Dunlop, J. S., McLure, R. J., & McLeod, D. J. 2017, MNRAS, 466, 3612
Bradley, L. D., Trenti, M., Oesch, P. A., et al. 2012, ApJ, 760, 108
Bradley, L. D., Zitrin, A., Coe, D., et al. 2014, ApJ, 792, 76
Bruzual, G., & Charlot, S. 2003, MNRAS, 344, 1000
Calvi, V., Trenti, M., Stiavelli, M., et al. 2016, ApJ, 817, 120
Calzetti, D., Armus, L., Bohlin, R. C., et al. 2000, ApJ, 533, 682
Chabrier, G. 2003, PASP, 115, 763
Chan, B. M. Y., Broadhurst, T., Lim, J., et al. 2017, ApJ, 835, 44
Coe, D., Zitrin, A., Carrasco, M., et al. 2013, ApJ, 762, 32
Ferguson, H. C., Dickinson, M., Giavalisco, M., et al. 2004, ApJL, 600, L107
Finkelstein, S. L. 2016, PASA, 33, e037
Finkelstein, S. L., Ryan, R. E., Jr., Papovich, C., et al. 2015, ApJ, 810, 71
Hashimoto, T., Laporte, N., Mawatari, K., et al. 2018, Natur, 557, 392
Hoag, A., Bradač, M., Trenti, M., et al. 2017, NatAs, 1, 0091
Holwerda, B. W., Bouwens, R., Oesch, P., et al. 2015, ApJ, 808, 6
Infante, L., Zheng, W., Laporte, N., et al. 2015, ApJ, 815, 18
Ishigaki, M., Kawamata, R., Ouchi, M., Oguri, M., & Shimasaku, K. 2018, ApJ, 854, 73
Laporte, N., Ellis, R. S., Boone, F., et al. 2017, ApJL, 837, L21
Mainali, R., Kollmeier, J. A., Stark, D. P., et al. 2017, ApJL, 836, L14
Merlin, E., Bourne, N., Castellano, M., et al. 2016, A&A, 595, A97
Oesch, P. A., Bouwens, R. J., Illingworth, G. D., et al. 2014, ApJ, 786, 108
Oesch, P. A., Bouwens, R. J., Illingworth, G. D., Labbe, I., & Stefanon, M. 2018, ApJ, 855, 105
Oesch, P. A., Brammer, G., van Dokkum, P. G., et al. 2016, ApJ, 819, 129
Oguri, M. 2010, PASJ, 62, 1017
Papovich, C., Dickinson, M., & Ferguson, H. C. 2001, ApJ, 559, 620
Paterno-Mahler, R., Sharon, K., Coe, D., et al. 2018, ApJ, 863, 154
Planck Collaboration, Aghanim, N., Arnaud, M., et al. 2011, A&A, 536, A26
Rigby, J. R., Bayliss, M. B., Gladders, M. D., et al. 2015, ApJL, 814, L6
Salmon, B., Coe, D., Bradley, L., et al. 2017, arXiv:1710.08930
Salmon, B., Papovich, C., Finkelstein, S. L., et al. 2015, ApJ, 799, 183
Salmon, B., Papovich, C., Long, J., et al. 2016, ApJ, 827, 20
Salpeter, E. E. 1955, ApJ, 121, 161
Schmidt, K. B., Treu, T., Trenti, M., et al. 2014, ApJ, 786, 57
Shibuya, T., Ouchi, M., & Harikane, Y. 2015, ApJS, 219, 15
Smit, R., Swinbank, A. M., Massey, R., et al. 2017, MNRAS, 467, 3306
Stark, D. P. 2016, ARA&A, 54, 761
Stark, D. P., Richard, J., Siana, B., et al. 2014, MNRAS, 445, 3200
Stark, D. P., Walth, G., Charlot, S., et al. 2015, MNRAS, 454, 1393
Williamson, R., Benson, B. A., High, F. W., et al. 2011, ApJ, 738, 139
Zheng, W., Postman, M., Zitrin, A., et al. 2012, Natur, 489, 406
Zitrin, A., Labbé, I., Belli, S., et al. 2015, ApJL, 810, L12
Zitrin, A., Zheng, W., Broadhurst, T., et al. 2014, ApJL, 793, L12